

# Spot Sizes on Sun-like Stars

S. K. Solanki,<sup>1</sup> and Y. C. Unruh<sup>2</sup>

<sup>1</sup> Max-Planck-Institut für Aeronomie, D-37191 Katlenburg-Lindau, Germany

<sup>2</sup> Astrophysics Group, Blackett Laboratory, Imperial College for Science, Technology and Medicine, London, SW7 2BW, United Kingdom

Accepted 4th Nov 2003; Received Aug 2003; in original form May 2003

## ABSTRACT

The total area coverage by starspots is of interest for a variety of reasons, but direct techniques only provide estimates of this important quantity. Sunspot areas exhibit a lognormal size distribution irrespective of the phase of the activity cycle, implying that most sunspots are small. Here we explore the consequences if starspot areas were similarly distributed. The solar data allow for an increase in the fraction of larger sunspots with increasing activity. Taking this difference between the size distribution at sunspot maximum and minimum, we extrapolate to higher activity levels, assuming different dependencies of the parameters of the lognormal distribution on total spot coverage. We find that even for very heavily spotted (hypothetical) stars a large fraction of the spots are smaller than the current resolution limit of Doppler images and might hence be missed on traditional Doppler maps.

**Key words:** sunspots, stars: spots, stars: late-type, stars: activity

## 1 INTRODUCTION

In recent years, an ever increasing number of spotted stars have been mapped using Doppler imaging. The maps reveal the surface distribution of starspots, which in general are large compared to even the largest sunspots. While Doppler images do a good job of catching starspots that modulate the line profile, it is extremely difficult to detect a background of small starspots more or less homogeneously distributed over the stellar surface. While TiO-band mapping still suffers from notable uncertainties (see Sec. 2), it should in principle be able to pick up non-modulating and homogeneous spot distributions. Typically, techniques using TiO bands to determine spot temperatures and surface areas tend to find larger covering fractions than Doppler imaging techniques (though see also Berdyugina (2002)). Such differences in apparent spot coverage only provide a hint for unresolved starspots. One star for which the distribution of spot sizes is known in great detail is the Sun. Bogdan et al. (1988) found the size distribution to be well represented by a lognormal function. This implies that the number of small sunspots is much larger than that of large spots. This supports the idea that there could be additional small, i.e. unresolved, starspots on more active stars as well. The total starspot coverage is of interest as a measure of stellar magnetic activity, in order to establish the proper ratio of starspot to stellar plage (Radick et al. 1998) and to obtain improved estimates of the total magnetic flux carried by the star (with the possible exception of Zeeman Doppler imaging where most of the magnetic signal appears to come from penumbral-type

structures, techniques of stellar magnetic field measurement mainly sample plage fields (Saar 1986; Solanki 1992)).

Here we explore hypothetical scenarios for extrapolating the solar spot-size distribution to activity levels typical for much more active stars. The basic assumption is that the size distribution of star spots can be described by a lognormal function, as in the case of sunspots. This assumption is not unreasonable since the magnetic fields on both the Sun and on more active cool stars are thought to be produced by a dynamo residing at the base of the convection zone (Petrovay 2001; Schüssler & Schmitt 2002). From there flux tubes carry the field to the solar surface. The fragmentation of these tubes during their passage through the convection zone is thought to give rise to the observed lognormal distribution (Bogdan et al. 1988). Lognormal distributions can, however, differ significantly from each other in their parameters.

In order to constrain these parameters for active stars we investigate the possible range of behaviour between solar activity minimum and maximum and use these to extrapolate to larger levels of activity. Hence we assume that the processes which lead to the flux-tube size distribution do not change qualitatively with increasing activity. Such an assumption has in the past helped to reproduce, e.g., the high latitudes of starspots (Schüssler & Solanki 1992; Schüssler et al. 1996; Schrijver & Title 2001), or the presence of active longitudes on the Sun and Sun-like stars Berdyugina & Usoskin (2003).

**Table 1.** A selection of RS CVn stars whose spot coverages have been determined using different techniques. The first column gives the name of the object, the second and third columns the surface and spot effective temperatures according to O’Neal, Neff & Saar (1998). The fourth column gives the inclination angle, usually taken from the Doppler imaging papers listed in Sec. 2.1. Note that not all groups agree on the spot temperatures and inclination angles.

Object	T <sub>star</sub>	T <sub>spot</sub>	inclination
II Peg	4750	3530	60°
EI Eri	5600	3700	46°
σ Gem	4600	3850	60°
DM UMa	4600	3570	55°
HD 199178	5350	3800	40°

## 2 DIFFERENT MAPPING TECHNIQUES

To our knowledge, TiO modelling has so far mainly been published for giant stars. One exception is Saar & Neff (1990), who calculate filling factors for 2 dwarf stars. As they do not give the epoch for their observations, comparison to Doppler maps is difficult. We therefore limit the discussion to 5 RSCVn stars for which spot covering fractions have been derived from (near) simultaneous data using different techniques. Tab. 1 lists the stars together with their effective and spot temperatures as well as the inclination angles of their rotation axes to the line of sight. Tab. 2 lists the spot covering fractions for the stars from Tab. 1.

The observations for the TiO *filling factors* have all been taken from Neff, O’Neal & Saar (1995); O’Neal, Saar & Neff (1996) and O’Neal, Neff & Saar (1998). Due to activity cycles and in some cases due to incomplete phase coverage, there are considerable variations in the filling factors measured for the same star by the same group, but at different times. In order to be able to compare them to the spot coverage fractions listed in columns 6 and 8 we converted them to a “minimum” and a “most likely” spot coverage. This is described in more detail later.

The measurements of the photometric spot coverages (column 6 in Tab. 2) are taken from Henry et al. (1995), Rodonò et al. (2000) and Padmakar & Pandey (1999) and are labelled (H+), R(+) and (PP), respectively, in column 7. The covering fractions derived from photometry by Henry et al. (1995) are lower limits as they have used the maximum light level during each individual observing period to represent the brightness of the unspotted star. If we use the brightness maxima over all of their observations, the areas need to be increased. While the exact increase depends amongst others on the spot geometry and the stellar and spot temperatures, we estimate that for σ Gem total surface coverages of about 6% are more typical than the values given by Henry et al. (1995). For II Peg we find that the surface coverage was more like 15% towards the end of 1989 as well as during 1992 September. Rodonò et al. (2000) give two different values for the spot coverage, one derived using a maximum entropy method, the other (higher) one with a Tikhonov regularisation. When they use the theoretical maximum light-level inferred from TiO band calculations (see Neff, O’Neal & Saar (1995) for more details), their spot

areas increased by 15% and 20% of the total surface area for the maximum entropy and Tikhonov maps respectively.

The last two columns of Table 2 give the surface coverage and the references for Doppler imaging determinations. The covering fractions are taken from Berdyugina et al. (1998) (B98+), Washuettl, Strassmeier & Collier-Cameron (1998) (W98+), Washuettl, Strassmeier & Collier-Cameron (2001) (W01+), Dempsey et al. (1992) (D92+)<sup>1</sup>, Hatzes (1993) (H93), Hatzes (1995) (H95) and Strassmeier et al. (1999) (S99+). Note that most Doppler maps do not give the spot coverage as a direct parameter, showing the stellar surface temperature rather than a spot filling factor. We were therefore only able to use a relatively small selection of Doppler maps where the authors had either given the spot coverage such as in as B98+, W98+/W01+ (priv comm) and D92+, or where the maps presented allowed realistic estimates.

Tab. 2 indicates that Doppler imaging and photometric light curve modelling tend to result in a smaller spot covering fraction than TiO modelling<sup>2</sup>. Both, photometric light-curve modelling and Doppler imaging are prone to underestimating spot areas. This is mainly because they are not very sensitive to rotationally invariant surface features, e.g., banded structures or low-level and small-scale distributed surface features. The current resolution limit of Doppler imaging is 3° to 5° in longitude, depending mainly on the star’s rotational velocity, the spectrograph resolution and the signal-to-noise ratio that can be achieved. To put this into context, we recall that the largest sunspots have diameters of about 1°.

In an ideal world where the spectral type of the unspotted parts of the target star were known with very high accuracy, or where the brightness and line profile of the star can be measured at a time when it is unspotted, the total spot area at other epochs can be estimated. Such prior knowledge, unfortunately, is in general not available. Furthermore, it is unclear whether rapidly rotating stars ever are free of spots.

TiO modelling is the youngest technique to determine the spot coverage and can be used for stars of any rotation velocity (see Neff, O’Neal & Saar (1995); O’Neal, Saar & Neff (1996) and O’Neal, Neff & Saar (1998) for more detail). Either the strength or the general shape of the TiO band heads is matched with a linear combination of template-star spectra at the effective stellar temperature and the spot temperature. In this way, the spot filling factor is determined. If more than one band head is observed it is possible to determine spot temperature and spot filling factor independently (provided the temperature response of the band heads is sufficiently different from each other). The location of the spots is not recovered. The filling factors are weighted for the limb darkening, but depending on the loca-

<sup>1</sup> The surface coverage for σ Gem derived by Dempsey et al. (1992) has been obtained using a variant of a line-bisector analysis rather than by Doppler imaging.

<sup>2</sup> Recent work has often combined Doppler imaging and photometric lightcurve modelling, showing that one and the same starspot distribution can reproduce both kinds of data. In some cases this has slightly increased the total spot coverage compared to Doppler maps alone (see, e.g., Unruh, Collier Cameron & Cutispoto 1995).

**Table 2.** Spot area coverages (for the total stellar surface) of the stars listed in Table 1 obtained with different techniques. The first column gives the name of the object, the second column the date of the observations. Columns three to five give the coverages obtained with the TiO modelling technique. Column three gives the range of filling factors, while columns four and five give estimates for the total surface coverage derived from the filling factors. Columns 6 and 7 give the total spot coverage derived from lightcurve modelling and the corresponding reference. The last two columns give the surface coverage and the references for Doppler imaging determinations. See text for more detail.

Object	date	TiO bands			Lightcurves		Doppler imaging	
		ff	coverage	minimum	coverage	reference	coverage	reference
[1]	[2]	[3]	[4]	[5]	[6]	[7]	[8]	[9]
II Peg	Oct 89	[43..55]	42	28	13; 12/21	H+; R+		
	Aug 92	[36..50]	37	23			10-15	B98+
	Sep 92	[43..56]	43	28	9; 13/23	H+; R+		
	Jan 95	[26..35]	25	16	12/21	R+	10-15	B98+
EI Eri	Mar 92	[23..36]	25	11				
	Jan 95	[<12..18]	13	5			$\simeq 3$	W98+
	Dec 95	[15..15]	13	5			$< 7$	W01+
$\sigma$ Gem	Mar 90	[14..26]	19	9	2	H+	2.9-5.4	D92+
	Feb 91	[27..33]	28	13	4	H+		
	Mar 92	[10..20]	14	6	3	H+	7	H93
	Jan 95	[3..14]	8	3				
	Dec 95	[15..30]	21	11	4.4	PP		
DM UMa	Jan 95	[30..35]	30	15			12	H95
HD 199178	Oct 89	[16..32]	20	8			$\simeq 6$	S99+
	May 89/90							

tion of the spots (e.g., a central circular spot, or spots close to the limb only), the area coverage can be about a factor of two smaller or larger than the listed filling factor.

We have therefore calculated two estimates for the area coverage of the stars based on the inclination of the star and the possible spans of surface coverages for a given filling factor as shown in figure 8 of O’Neal, Saar & Neff (1996). The first estimate (listed in column 4 of Tab. 2) is calculated under the assumption that the filling factor is just the fractional spot coverage. For the second estimate (listed in column 5 of Tab. 2) we try and estimate a minimum coverage assuming that the spots are at disk centre where they produce the largest contribution.

For both estimates we use the mean filling factor  $(ff_{\max} + ff_{\min})/2$  as a starting point ( $ff_{\max}$  and  $ff_{\min}$  are the largest and smallest filling factors observed during a given observing season). To obtain the minimum spot coverage we reduce the filling factors according to the graphs for disk-centre spots shown in figure 8 of O’Neal, Saar & Neff (1996). This reduction is typically of the order of 50%, but depends on the value of the filling factor.

The average and minimum covering fractions that are obtained in this way are in fact not the covering fractions with respect to the total stellar surface, as the polar region that is pointing away from the observer is never visible. As the covering fractions calculated for Doppler imaging and also lightcurve modelling assume that the invisible part of the star is devoid of structure, we multiply the mean and minimum coverages with a factor of  $(1 + \sin i)/2$  and so recover the values listed in columns 4 and 5 of Tab. 2. Apart from the conversion from filling factor to surface spot covering, further errors in the TiO-band modelling can be introduced because of mismatches between the template star atmospheres and the actual stellar atmospheres. Note that TiO modelling assumes that stellar spectra are not affected

by magnetic activity beyond the strengths of the molecular features. This is clearly a simplification and adds uncertainty to the spot coverage fractions deduced by this technique.

### 3 SPOT DISTRIBUTIONS ON THE SUN

Bogdan et al. (1988) measured the size distribution of the sunspot umbral areas recorded at Mt Wilson between 1921 and 1982. They found that the size distribution could be well fitted with a lognormal distribution of the form

$$\frac{dN}{dA} = \left( \frac{dN}{dA} \right)_m \exp \left( -\frac{(\ln A - \ln \langle A \rangle)^2}{2 \ln \sigma_A} \right). \quad (1)$$

This is valid for umbral areas  $A_u$  larger than  $A_{\min} = 1.5 \times 10^{-6} A_{1/2\odot}$ , where  $A_{1/2\odot} = 2\pi R_{\odot}^2$  is the surface area of the visible solar hemisphere. Note that the total area of a sunspot  $A_s$  is the sum of the umbral area  $A_u$  and the much larger penumbral area  $A_p$ . Typical ratios of penumbral to umbral area vary between about 3 and 5 (Steinegger et al. 1990; Brandt, Schmidt & Steinegger 1990; Beck & Chapman 1993). In the following we assume that the penumbra is about 4 times larger than the umbra, so that  $A_s = 5A_u$ .

The three free parameters that have to be determined by observations are  $(dN/dA)_m$ , i.e. the maximum value reached by the distribution,  $\langle A \rangle$ , the mean sunspot umbral area and  $\sigma_A$ , a measure for the width of the lognormal distribution. If all area measurements are taken into account, these parameters take on the values (in units of  $10^{-6} A_{1/2\odot}$ ) of  $(dN/dA)_m = 9.4$ ,  $\sigma_A = 4.0$  and  $\langle A \rangle = 0.55$ . Bogdan et al. (1988) show that the same distribution can fit data from different cycles and that only variations in the value of  $(dN/dA)_m$  are statistically significant.

**Table 3.** Variations in  $\sigma_A$  for a fixed  $\langle A \rangle$  of 0.57. The first column labels the cycle activity: “all” indicates that all available data were fitted; “max” and “min” are for data taken in the years bracketing solar cycle maximum and minimum respectively; “max+” and “min+” also include the ascending respective descending phase of the cycle. The second column gives the fit for  $(dN/dA)_m$ , the third and forth columns give the values for  $\sigma_A$  and its standard deviation respectively.

cycle	$(dN/dA)_m$	$\sigma_A$	$\Delta\sigma_A$
[1]	[2]	[3]	[4]
all	9.21	3.95	0.04
max	13.56	4.02	0.05
max+	11.51	4.04	0.04
min	3.09	3.75	0.15
min+	4.99	3.71	0.07

#### 4 FITS TO THE SUNSPOT NUMBER DISTRIBUTION DURING DIFFERENT PHASES OF THE SOLAR CYCLE

While Bogdan et al. (1988) show that it is possible to fit the sunspot umbral size spectrum with the same distribution, the best-fit distributions are marginally different between sunspot maximum and minimum. This difference between activity maximum and minimum is small, but a weighting towards larger spots could become important if we were to extrapolate to higher activity levels such as the activity levels observed on the stars listed in Tab. 1.

In the following sections we explore what variations in  $\sigma_A$  and  $\langle A \rangle$  are consistent with the solar data and what these would imply for the spot coverage of more active stars. As this depends on the number of free parameters of the fits, we separately investigate 2-degree fits with either  $\langle A \rangle$  or  $\sigma_A$  fixed and a 3-degree fit where  $\langle A \rangle$ ,  $\sigma_A$  and  $(dN/dA)_m$  are all allowed to vary simultaneously.

##### 4.1 Fits with fixed $\langle A \rangle$

The initial fits involved varying only  $\sigma_A$  and  $(dN/dA)_m$ . In the first instance we obtained a fit using the logarithmic form of Eq. 1. Because of the logarithm, however, the errors are no longer normally distributed, so that there is no easy way to establish confidence limits. In order to obtain a reasonable estimate for the 1- $\sigma$  deviation, we calculated the value of  $\chi^2$  in the region surrounding the original fit (now using the non-logarithmic form, i.e. Eq. 1). We hence have a 2-dimensional region given by  $(dN/dA)_m$  and  $\sigma_A$  where contours of constant  $\chi^2$  describe ellipses. The constant- $\chi^2$  contours can be used to define a 1- $\sigma$  confidence region. For two degrees of freedom, the difference in  $\chi^2$  between this region and the best fit is 2.3. The value for  $(dN/dA)_m$ ,  $\sigma_A$  and the deviation on  $\sigma_A$  are given in Tab. 3. In all cases the original “logarithmic fit” lies within the 1- $\sigma$  contour. All fits listed are for  $\langle A \rangle = 0.57$ .

Note that the fits to the data taken during solar minimum when the number of sunspots on the disc is very small, are much less well constrained than those taken during maximum. As a consequence, the 1- $\sigma$  deviation at solar minimum is three times larger than at solar maximum. To achieve statistically more meaningful fits, we also considered a combined data set of solar minimum and the descending phase of

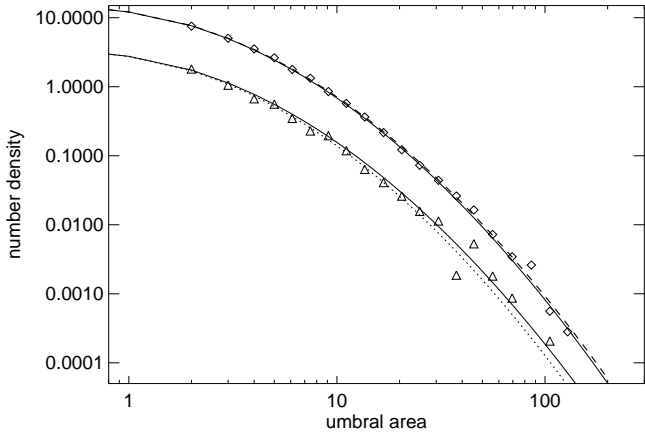


**Figure 1.** Plot of the spot number density as a function of umbral area (in units of  $10^{-6}$  solar hemisphere area) according to Bogdan et al. (1988) and lognormal fits to the data. The diamonds show the number density at solar maximum, the triangles the number distribution at solar minimum. The solid lines are the best fit for all data sets (i.e. row 1 of Tab. 3), multiplied by the maximum value of the distribution at maximum and minimum. Also shown are the best fits to data taken during solar maximum (dashed line) and solar minimum (dotted line, rows 2 and 4 of Tab. 3 respectively). All fits are for varying  $\sigma_A$  with  $\langle A \rangle$  fixed at 0.57.

the cycle (here labelled min+) and of solar maximum combined with the ascending phase of the cycle (labelled max+). While the best fits at solar minimum and maximum only deviate by about  $2 \Delta\sigma_A$ , the best fits at phase min+ and max+ differ by 4 to 5  $\Delta\sigma_A$ . Some of the fits for solar minimum and maximum are shown in Fig. 1 along with the spot number distribution at solar minimum and solar maximum taken from Bogdan et al. (1988). This shows that the distribution at solar minimum and maximum are indeed similar.

##### 4.2 Fits with fixed $\sigma_A$

The fits for varying values of  $\langle A \rangle$  and  $(dN/dA)_m$  were obtained in a similar manner to the ones for varying  $\sigma_A$ . Here we fixed  $\sigma_A$  to be 4.0 and again looked for constant  $\chi^2$ -difference contours at 2.3 for the 1- $\sigma$  confidence limits. We find that  $\langle A \rangle$  for the best fits varies between 0.49 and 0.58 for solar minimum and solar maximum respectively. The obtained values of  $\langle A \rangle$  are listed in Tab. 4.

While varying  $\sigma_A$  increases the width of the lognormal distribution, varying  $\langle A \rangle$  shifts the distribution towards larger  $A_u$ . Over the range of measured sunspot umbral sizes both methods yield equally good fits. The implications for small spots are, however, rather different. This is illustrated in Fig. 2 where the (normalised) lognormal distributions for fixed  $\sigma_A$  and for fixed  $\langle A \rangle$  at solar minimum and maximum are compared. The solid lines show the fits at solar minimum. The dashed line for varying  $\langle A \rangle$  shows the shift towards higher umbral sizes,  $A_u$ . The dot-dashed line reveals the broader distribution obtained for a larger value of  $\sigma_A$ . Note that the umbral areas measured by Bogdan et al. (1988) range from about 2 to 100. In this range, varying  $\sigma_A$  or  $\langle A \rangle$  gives an equivalent goodness-of-fit.

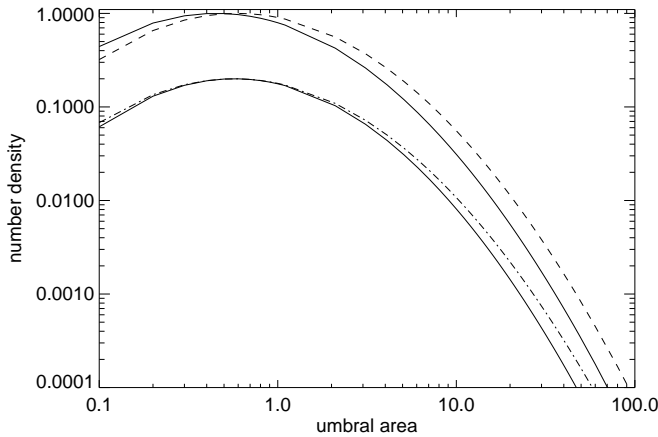


**Figure 2.** The lognormal fits to the sunspot umbral distributions at solar minimum (solid lines) and maximum (broken lines). The two uppermost lines show the fits for varying  $\langle A \rangle$ , the lower lines for varying  $\sigma_A$ . To bring out the small differences, we have taken the extreme values on the  $1-\sigma$  contours. All fits have been normalised. For clarity the varying- $\sigma_A$  fits have been offset.

**Table 4.** Variations in  $\langle A \rangle$  for fixed  $\sigma_A$ . The first column is as in the previous table and indicates the activity level. The second column gives  $(dN/dA)_m$  and the third and forth columns give  $\langle A \rangle$  and its  $1-\sigma$  deviation.

cycle [1]	$(dN/dA)_m$ [2]	$\langle A \rangle$ [3]	$\Delta\langle A \rangle$ [4]
all	9.40	0.56	0.01
max	13.37	0.58	0.01
max <sup>+</sup>	11.32	0.58	0.01
min	3.45	0.50	0.05
min <sup>+</sup>	5.67	0.49	0.02

Hence the difference in the fits mainly affects the number of pores, dark structures that are on average smaller than sunspots.

### 4.3 Variations in $\langle A \rangle$ and $\sigma_A$

If all three parameters are allowed to vary, the  $1-\sigma$  confidence region is inside an ellipsoid whose surface has a value of  $\chi^2$  that is higher by 3.5 than the minimum value of  $\chi^2$ . However, the data are not sufficient to constrain the three fit parameters very tightly and the  $1-\sigma$  deviations increase by more than a factor of 5 compared to the 2-degree fits presented in the previous section. Furthermore, the relationship between the  $\langle A \rangle$  and  $\sigma_A$  parameters and the cycle characteristic is no longer straightforward. Going from solar minimum to solar maximum in the previous sections implied larger values for  $\langle A \rangle$  or  $\sigma_A$ . If  $\langle A \rangle$  and  $\sigma_A$  are both allowed to vary, we tend to still get larger values for  $\langle A \rangle$  (i.e., a shift towards larger mean spot sizes), though at the expense of  $\sigma_A$  that now decreases (see columns 3 and 4 of Tab. 5). This suggests, rather unexpectedly, a narrower distribution for higher levels of activity.

When we look at the parameters within the  $1-\sigma$  confidence regions, the picture becomes less clear, as there is

**Table 5.** Variations in  $\langle A \rangle$  and  $\sigma_A$ . The first column again lists the phase of the activity cycle. The second column gives the best-fit values for  $(dN/dA)_m$ . Columns three and four gives the best-fit value of  $\sigma_A$  along with its deviation. The fifth and sixth columns list  $\langle A \rangle$  along with its deviation.

cycle [1]	$(dN/dA)$ [2]	$\sigma_A$ [3]	$\Delta\sigma_A$ [4]	$\langle A \rangle$ [5]	$\Delta\langle A \rangle$ [6]
all	9.4	4.0	0.3	0.56	0.10
max	12.4	3.8	0.3	0.64	0.09
max <sup>+</sup>	10.9	3.9	0.3	0.61	0.07
min	4.2	4.6	3.1	0.39	0.19
min <sup>+</sup>	6.4	4.3	0.8	0.43	0.10

overlap between the solar-maximum and solar-minimum parameters. Most parameters suggest that the distribution at solar maximum is steeper as described above, but there are also some choices where the distribution at solar maximum is flatter, but shifted towards smaller-sized spots. This makes it rather difficult to pick scaling parameters (see Sec. 5.3 for more details).

## 5 EXTRAPOLATIONS TO MORE ACTIVE STARS

In addition to  $(dN/dA)$  given by Eq. 1, the following quantities are of importance for the current analysis:  $A(dN/dA)$ ,  $S_N(A)$  and  $S_A(A)$  (see also Solanki 1999).  $S_N(A)$  and  $S_A(A)$  are the integrals over  $(dN/dA)$  and  $A(dN/dA)$ , respectively, both being normalised to their maximum values:

$$\begin{aligned} S_N(A) &= \int_{A_{\min}}^A \frac{dN}{dA'} dA' \Big/ \int_{A_{\min}}^{A_{\max}} \frac{dN}{dA'} dA' \\ &= \int_{A_{\min}}^A dN/N_{\text{tot}}, \end{aligned} \quad (2)$$

$$\begin{aligned} S_A(A) &= \int_{A_{\min}}^A A' \frac{dN}{dA'} dA' \Big/ \int_{A_{\min}}^{A_{\max}} A' \frac{dN}{dA'} dA' \\ &= \int_{A_{\min}}^A A' dN/A_{\text{tot}}, \end{aligned} \quad (3)$$

$S_N(A)$  describes the relative contribution of spots with area between  $A_{\min}$  and  $A$  to the total number of spots, while  $S_A(A)$  gives the relative contribution of these spots to the total area covered by all spots on the solar or stellar surface. The latter is hence the key quantity to compare with stellar observations of different types such as molecular line strengths, which give a measure of the total area covered by spots,  $A_{\text{tot}}$  (relative to the stellar surface area), and Doppler images, which provide information mainly on the spots above a certain size. Example plots of  $(dN/dA)$ ,  $A(dN/dA)$ ,  $S_N(A)$  and  $S_A(A)$  for different activity levels are shown in Figs 3 and 4, and will be discussed in the following section.

### 5.1 Spot coverage for varying $\sigma_A$

Having only two points to extrapolate from, we have in principle a large possible range of scalings. In the fol-

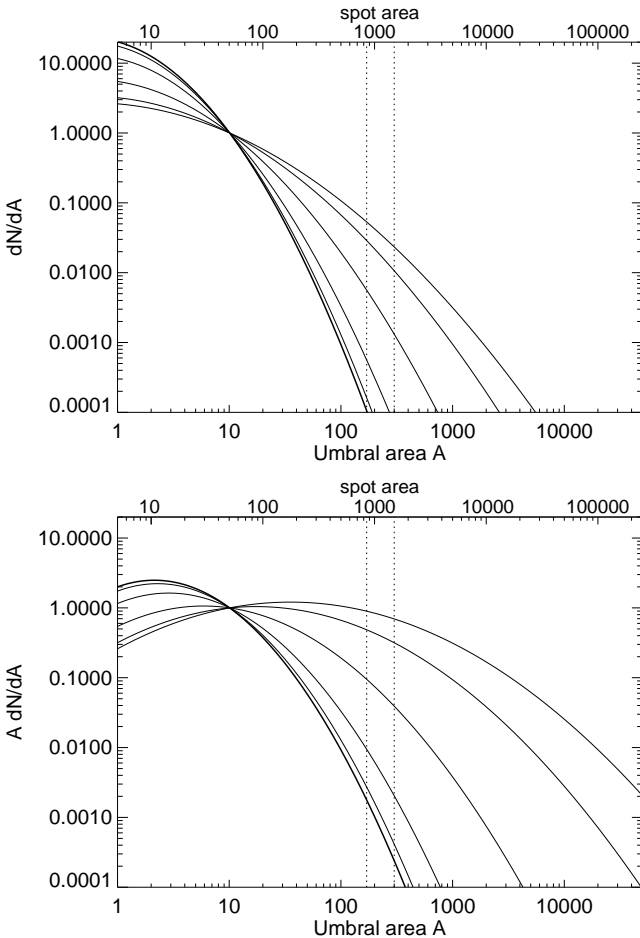


**Figure 3.** Plots of number and size distribution ( $dN/dA$ ) (top) and  $A(dN/dA)$  (bottom) of sunspot umbrae as a function of spot umbral area  $A_u$  in units of  $10^{-6} A_{1/2\odot}$ . It is assumed that  $n_\sigma = 1$ , i.e.,  $\sigma_A$  is proportional to spot surface coverage. The distributions for the quiet Sun are represented by the thick lines. The next line towards the right shows ( $dN/dA$ ) ( $A(dN/dA)$  for the lower plot) at solar maximum, while the lines further to the right illustrate the extrapolations to more active stars, up to a hypothetical star where about 75% of one hemisphere is covered by spots (see Tab. 6 for a list of parameters). The distributions have been normalised to their values at an umbral area of  $A = 10 \times 10^{-6} A_{1/2\odot}$ . The two dotted lines at  $170 \times 10^{-6} A_{1/2\odot}$  and  $300 \times 10^{-6} A_{1/2\odot}$  indicate resolution limits of Doppler imaging (see text for more detail).

lowing, we require that  $\sigma_A$  scales with stellar activity as parameterised by the spot covering fraction, i.e.,  $\sigma_A = \sigma_A^0 + \Delta_\sigma (A_{\text{spot}}/A_*)^{n_\sigma}$ . The main open question concerns the choice of  $n_\sigma$ . Plots of solar magnetic activity proxies, such as Ca II H & K or the 10.7 cm radio flux versus spot coverage show very large scatter and it is not clear how the spot size distribution scales with magnetic activity. We therefore take the approach of choosing values of  $n_\sigma$ , carrying out the analysis and from a comparison with Doppler imaging and TiO results deciding whether our choice is reasonable. Exponents  $n_\sigma$  with values between 0.5 and 1.0 yield such results and will be discussed in the following.

For the extrapolations shown here,  $\langle A \rangle$  is kept fixed at 0.57, while we use the best-fit values of  $\sigma_A = 3.75$  and

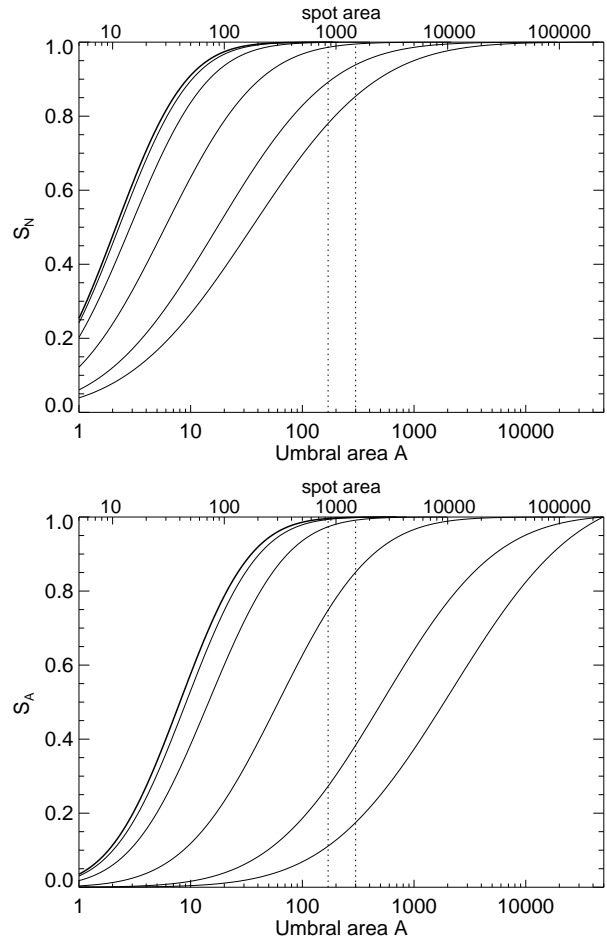


**Figure 4.** Plots of the integral functions  $S_N$  (top) and  $S_A$  (bottom) as a function of umbral area  $A$ . The thicker lines show  $S_N$  and  $S_A$  for the quiet Sun, while lines further to the right are for (linearly) increasing values of  $\sigma_A$ . See text for the definition of  $S_N$  and  $S_A$  and Tab. 6 for a list of plot parameters.

$\sigma_A = 4.0$  at solar minimum and maximum respectively. The values for  $(dN/dA)_m$  at solar minimum and maximum were adjusted so that the spot covering fraction at solar minimum and maximum were 0.03% and 0.3% respectively. Having preset the above parameters and picked a value for the exponent  $n_\sigma$ , we determine  $\sigma_A^0$ , the width of the lognormal distribution in the limit of zero spot coverage and  $\Delta_\sigma$ , the increase in the width with increasing activity.

The solution for each activity level is then found by presetting  $(dN/dA)_m$  and guessing a spot coverage  $A_{\text{spot}}/A_*$ , and hence a new  $\sigma_A$ . Eq. 1 is then integrated to obtain a new spot coverage. This process is iterated until the calculated and input spot coverages agree. For exponents,  $n_\sigma$ , below about 0.7 this is straightforward with each next-higher value of  $(dN/dA)_m$  yielding a solution with a higher spot coverage. For steeper exponents, there is a threshold value for  $(dN/dA)_m$  beyond which no solutions can be found. But below the threshold value there are generally two solutions, one for a low surface coverage and hence low  $\sigma_A$ , and one with a much higher surface coverage. This can be seen from Tab. 6 where for  $n_\sigma = 1$  the different parameters of the lognormal distribution are listed along with the calculated spot cov-

**Table 6.** Spot covering fractions and the proportion of spots above the “Doppler imaging threshold” for  $\sigma_A$  increasing linearly with stellar activity (stellar activity is parametrised with the spot surface coverage). Rows 2 and 3 list the values for  $\sigma_A$  and  $(dN/dA)_m$ . The forth row gives the fractional spot coverage of one hemisphere. The fifth and sixth rows give the fraction of spots that can be seen on a Doppler map with  $4^\circ$  and  $3^\circ$  resolution respectively (note that row 5 (or 6) has to be multiplied with row 4 so as to obtain the fractional spot coverage that would be deduced from a Doppler image).

solar:	min	max				
$\sigma_A$	3.75	4.00	5.04	10.4	30.3	62
$(dN/dA)_m$	4.5	38.5	106	106	41.2	20.8
$A_{\text{spot}}/A_*$	0.0003	0.003	0.014	0.07	0.28	0.62
$A_{\text{DI}}/A_{\text{tot}}$	0.003	0.003	0.010	0.15	0.61	0.83
	0.006	0.008	0.027	0.25	0.73	0.89

ering fractions for different activity levels. The umbral-size distributions for the same parameters are plotted in Fig. 3, the different lines correspond to the columns of Tab. 6. The quiet-Sun behaviour is indicated by the thickest and leftmost line. The next line to the right is for solar maximum, with  $\sigma_A$  increasing from 3.75 to 4.0 between solar minimum and maximum as outlined above. The two vertical dotted lines gives an indication of the currently achievable resolution with Doppler imaging. Only spots with areas larger than indicated by the dotted lines can be picked up.

If we ask what fraction of the stellar surface is covered by spots larger than a given size, we have to consider the integral  $S_A$ . This integral is shown for the parameters given in Tab. 6 in the bottom plot of Fig. 4. The top graph of Fig. 4 shows the integral  $S_N$ . We have assumed that the current resolution limit for Doppler imaging is around  $3^\circ$  or  $4^\circ$ . For circular features this is equivalent to effective surface areas of 340 and  $600 \times 10^{-6} A_{1/2\odot}$ . The effective area does not correspond to the actual area of a starspot, since the latter is probably composed of an umbra which produces a large contrast, and a penumbra, which produces a smaller contrast per unit area. Hence the effective area lies between the area of the starspot and that of its umbra. To quantify this effective area better we have carried out some tests using a Doppler imaging code that is based on a spot-filling factor approach (see e.g. Collier Cameron & Unruh 1994). They show that the relative contribution of a spot umbra at 4500 K and a penumbra at 5400 K that is four times larger than the umbra is similar<sup>3</sup>. Such a penumbra-to-umbra area ratio is typical of sunspots (see Solanki (2003) for an overview). We therefore assume that the umbral area of the smallest resolvable spot is  $170 \times 10^{-6} A_{1/2\odot}$ , respectively  $300 \times 10^{-6} A_{1/2\odot}$ , as indicated by the dotted lines in Figs 3, 4 and 6. This corresponds to total spot areas of  $850 \times 10^{-6} A_{1/2\odot}$  and  $1500 \times 10^{-6} A_{1/2\odot}$ , i.e., spot diameters of approximately  $5^\circ$  and  $6^\circ$ .

The percentage of spots that will be picked up by Doppler imaging is listed in the bottom two rows of Tab. 6 for  $\sigma_A$  increasing linearly with the spot surface coverage, i.e.  $n_\sigma = 1$ . The individual columns correspond to the lines

<sup>3</sup> This is of course just a rough estimate as the exact ratio depends on the particular line that is used for the mapping.

**Table 7.** Spot covering fractions and the proportion of spots above the “Doppler imaging threshold” for  $\sigma_A$  increasing as the square-root of stellar activity (see Tab. 6 for explanations of the symbols).

solar:	min	max				
$\sigma_A$	3.75	4.00	4.47	5.24	6.6	9.6
$(dN/dA)_m$	4.5	38.5	155	396	796	1393
$A_{\text{spot}}/A_*$	0.0003	0.003	0.015	0.06	0.19	0.78
$A_{\text{DI}}/A_{\text{tot}}$	0.004	0.004	0.005	0.01	0.04	0.12
	0.007	0.009	0.015	0.03	0.08	0.22

drawn in Fig. 4. It turns out that for very large  $\sigma_A$  characterising wide lognormal spot distributions a substantial fraction of spots that are present on the stellar surface are indeed seen on the Doppler maps. We note that this is not the case for slower scaling laws ( $n_\sigma < 0.7$ ), where even for very large covering fractions less than half the spots are picked up on the Doppler maps. Tab. 7 lists the spot coverage and pick-up fraction for  $n_\sigma = 0.5$ .

Different scaling laws are also contrasted in Fig. 5 where the spot area seen on Doppler images is plotted against the actual spot area. The solid lines are for  $n_\sigma = 1$ , the dashed lines for  $n_\sigma = 0.5$  and the dot-dashed lines for the intermediate case of  $n_\sigma = 0.75$ . The symbols denote data points from Tab. 2 where simultaneous Doppler maps and TiO filling factors were available. The stark difference between the square-root and linear scaling laws is due to the pronounced shape-change of the lognormal distribution for a linear increase. This results in a greater fraction of large spots compared to “average” spots. The number of smaller spots of course also increases, but this is negligible because of their small contribution to the total spot area. In the square-root scaling, the increase in the total spot area is achieved mainly by increasing the height of the distribution rather than its width as indicated by the ever increasing  $(dN/dA)_m$  in Tab. 7. This produces a much slower change in the fraction of large to average-size spots so that only a very limited number of spots fall above the detection threshold. It is clear from Tabs 6 and 7 and from Fig. 5 that the curves for  $n_\sigma = 1$  and 0.5 lie sufficiently far apart to encompass most of the data points. In fact, we find that most data points can be accommodated with  $n_\sigma$  between 0.75 and 1.

## 5.2 Spot coverage for varying $\langle A \rangle$

We now keep  $\sigma_A$  fixed and extrapolate by allowing  $\langle A \rangle$  to vary. The assumption in this case is that as we move from solar minimum through solar maximum and on to more active stars, the mean spot size,  $\langle A \rangle$ , increases, thereby shifting the distribution towards higher values of  $A$ . The mean spot size increases with spot coverage according to  $\langle A \rangle = \langle A \rangle^0 + \Delta_A (A_{\text{spot}}/A_*)^{n_A}$ . Again, the value for  $n_A$  is the biggest unknown. Here we illustrate the results for the same values as for  $n_\sigma$ , i.e. we assume  $n_A = 0.5$ , 0.75 and 1.0. While the fits to the solar minimum and maximum distribution with either varying  $\sigma_A$  or  $\langle A \rangle$  are very similar (see Fig. 2), the distributions differ strongly for more active stars. This is illustrated in Fig. 6 where the number and size distributions for increasing  $\langle A \rangle$  have been plotted. Note the much

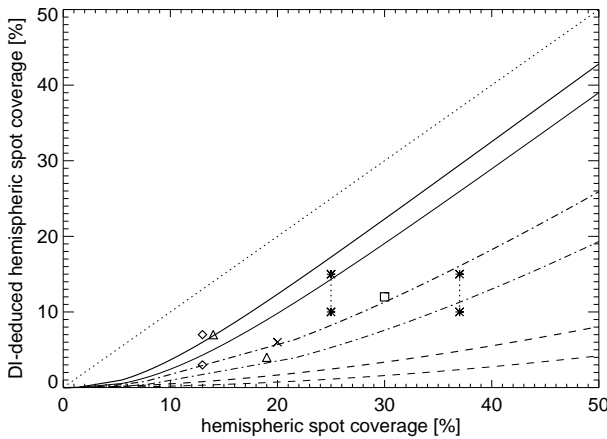


**Figure 5.** Plots of the surface coverage deduced from Doppler imaging as a function of actual surface coverage. The solid lines are for  $\sigma_A$  increasing linearly with the surface-spot coverage ( $n_\sigma = 1$ ), the dot-dashed lines are for  $n_\sigma = 0.75$  and the dashed lines for  $n_\sigma = 0.5$ . The lower-lying thin lines are for a resolution threshold of  $4^\circ$ , while the upper heavier lines are for a resolution threshold of  $3^\circ$ . The dotted line is plotted as a help to mark out a situation where all spots present on the star would also appear on the Doppler map. Also shown are some data points from Tab. 2 where simultaneous Doppler images and TiO filling factor estimates are available. These TiO estimates were used to represent the spot coverage of one hemisphere. The points plotted are for II Peg (stars), EI Eri (diamonds),  $\sigma$  Gem (triangles), DM UMa (square) and HD 199178 (cross).

**Table 8.** Spot covering fractions and the proportion of spots above the “Doppler imaging threshold” for  $\langle A \rangle$  increasing linearly with stellar activity, as parametrised with the spot surface coverage. See Tab. 6 for a description of the symbols.

solar:	min	max				
$\langle A \rangle$	0.50	0.58	1.36	3.2	9.1	16.7
$(dN/dA)_m$	5	37	66	37	15	8
$A_{\text{spot}}/A_*$	0.0003	0.003	0.03	0.09	0.29	0.54
$AD_{\text{I}}/A_{\text{tot}}$	0.001	0.003	0.015	0.07	0.27	0.46
	0.005	0.009	0.042	0.15	0.45	0.65

smaller number of large spots for the “shifted” distribution compared to the “widened” distribution shown in Fig. 3.

The extrapolations for  $\langle A \rangle$  were carried out in a similar manner as described in the previous section, with  $\langle A \rangle = \langle A \rangle^0 + \Delta_A (A_{\text{spot}}/A_*)^{n_A}$ . The fixed values are  $\sigma_A = 4.0$  for all fits,  $\langle A \rangle = 0.50$  at solar minimum and  $\langle A \rangle = 0.58$  at solar maximum. Some example parameters and results are listed in Tab. 8. We find that the “shift” of the lognormal distribution towards larger  $A$  is less efficient in creating spots that are large enough to be picked up on Doppler maps. This can be seen by comparing Figs 5 and 7, where the spot covering fractions that would be seen on a typical Doppler map are plotted against the actual spot covering fraction. On both plots the thicker lines are for a resolution of  $3^\circ$ , while the thinner (and lower-lying) lines are for a resolution of  $4^\circ$ . Fig. 7 also shows the spot covering fractions that would be picked up for  $n_A = 0.75$  (dot-dashed lines) and  $n_A = 0.5$  (dashed lines). Note that the pick-up rates for  $n_A = 0.5$

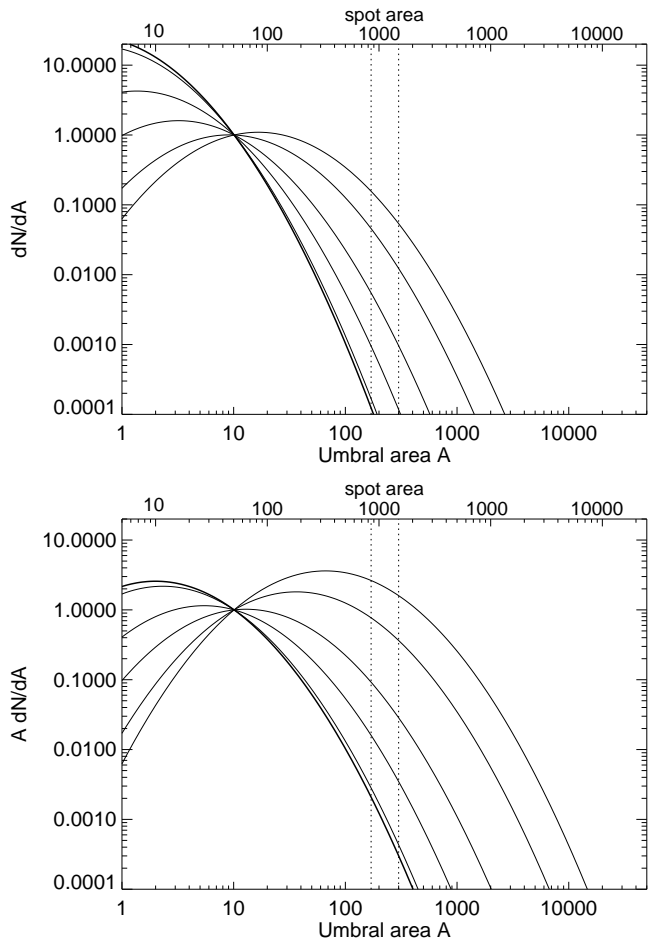


**Figure 6.** Plots of number and size distribution ( $dN/dA$ ) (top) and  $A(dN/dA)$  (bottom) of sunspot umbrae as a function of spot umbral area. The distributions for the quiet Sun are represented by the thick lines. The next line towards the right corresponds to solar maximum, while the lines further to the right illustrate the extrapolations to more active stars where  $\langle A \rangle$  increases linearly with the total spot coverage. See Fig. 3 for a comparison with extrapolations in  $\sigma_A$  and Tab. 8 for a list of the parameters used for this plot.

are almost one order of magnitude smaller than those predicted for a linear increase in  $\langle A \rangle$ . Our calculations suggest that if, indeed, the lognormal distribution scales with mean spot size, then some spot clumping is needed to explain the relatively high pick-up rates on the Doppler maps. Starting from solar observations as well as from observations of active longitudes on rapidly rotating stars, some amount of spot clumping is in fact expected.

### 5.3 Spot covering for varying $\sigma_A$ and $\langle A \rangle$

When both,  $\sigma_A$  and  $\langle A \rangle$ , are allowed to vary between solar minimum and maximum, we get the somewhat curious situation that, for the best fits, only the value for  $\langle A \rangle$  increases between minimum and maximum, while the value of  $\sigma_A$  decreases (see Tab. 5). Extrapolating from there we can reproduce the results found in Sects 5.1 and 5.2, i.e., obtain curves similar to those plotted in Figs 5 and 7. Since there are now two free parameters ( $n_\sigma$  and  $n_A$ ) compared to

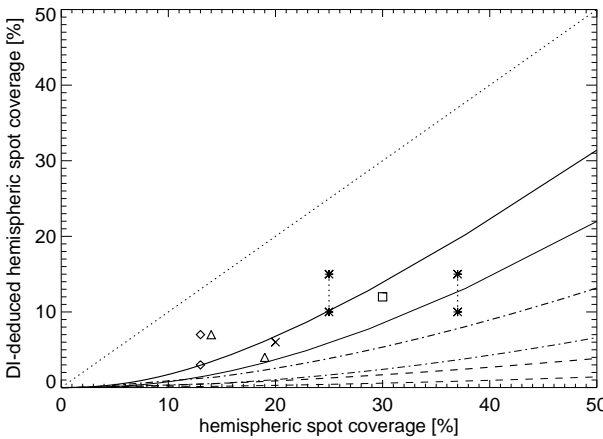


**Figure 7.** Plots of the surface coverage deduced from Doppler imaging as a function of actual surface coverage for scaling laws with  $\langle A \rangle = \langle A \rangle^0 + \Delta_A (A_{\text{spot}}/A_*)^{n_A}$ . The solid, dot-dashed and dashed lines are for exponents,  $n_A$ , of 1.0, 0.75 and 0.5 respectively. The lower-lying thin lines are for a resolution threshold of  $4^\circ$ , the upper heavier lines for a resolution threshold of  $3^\circ$ . The symbols are data points from Tab. 2 (see caption of Fig. 5 for more detail).

only one in the previous sections, this is not surprising and we do not learn anything new. Therefore we refrain from discussing these extrapolations in detail.

## 6 DISCUSSION AND CONCLUSIONS

We consider some of the consequences if spot sizes follow a lognormal distribution as on the sun. Bogdan et al. (1988) proposed that the passage of magnetic flux tubes from the dynamo to the stellar surface through the turbulent convection zone leads to a certain fragmentation of the flux, producing a lognormal distribution of umbral areas (flux-tube cross-sections). In this picture a significant fraction of the total starspot area of any star is in the form of starspots below the resolution limit of Doppler images. The sunspot-size distribution is consistent with a shift towards larger spots at solar activity maximum. We have used the possible range in the solar parameters to extrapolate to higher activity levels in different ways and have compared the resulting fractional spot areas that can be resolved by Doppler imaging. This has been done assuming that the starspots are randomly distributed on the stellar surface, which implies that most starspots resolved by Doppler imaging are single spots. Hence we assume that starspots do not clump. If they clump together as in solar active regions then Doppler images detect a larger fraction of the starspots than suggested by our analysis.

Recent calculations of Berdyugina (2002) suggest that at least for the RS CVn star II Peg, spectral synthesis of the TiO band reproduces the observations of these molecular lines without requiring starspots in addition to those present on the corresponding Doppler image. If starspot distributions on RS CVn stars are indeed log-normal and follow a sun-like pattern, this result would suggest that the starspots are tightly clumped and that the starspots resolved

by Doppler imaging are actually conglomerates of smaller spots. The low photospheric temperature of II Peg (Table 1), however, means that CN lines blending the analysed TiO band are also present in the spectrum of the immaculate star (Berdyugina, priv. comm.). Due to uncertainties in the exact temperature there are also some uncertainties in the above result and further such calculations for hotter stars would be of great interest.

If larger spots increase in number more rapidly than smaller spots as stars become more active, we also expect starspots as a whole to be more numerous relative to smaller magnetic flux tubes, i.e., bright magnetic elements. The “switch-over” between activity-bright and activity-dark stars seen with increasing activity level (Radick et al. 1987; 1990; 1998; Lockwood et al. 1992) fits well into this, as does the strong increase of spot area relative to facular area from solar activity minimum to maximum (Chapman, Cookson & Dobias 1997). The fact that model calculations based on extrapolations from solar values do reproduce the switch-over at about the correct activity level (Knaack 1998), supports our general approach of extrapolating the size distribution of spots from the Sun to more active stars.

## ACKNOWLEDGMENTS

The authors would like to thank T. Bogdan for digging out his notes and providing us with his data on the spot-size distributions.

## REFERENCES

- Beck J. G., Chapman G. A., 1993, *Solar Phys.*, 146, 49
- Berdyugina S. V., Usoskin I. G., 2003, *A&A*, submitted
- Berdyugina S. V., Berdyugin A. V., Ilyin I., Tuominen I., 1998, *A&A*, 340, 437
- Berdyugina S. V., 2002, *Astron. Nachr.*, 323, 192
- Bogdan T. J., Gilman P. A., Lerche I., Howard R., 1988, *ApJ*, 327, 451
- Brandt P. N., Schmidt W., Steinegger M., 1990, *Solar Phys.*, 129, 191
- Chapman G. A., Cookson A. M., Dobias J. J., 1997, *ApJ*, 482, 541
- Collier Cameron A., Unruh Y. C., 1994, *MNRAS*, 269, 814
- Dempsey R. C., Bopp B. W., Strassmeier K. G., Granados A. F., Henry G. W., Hall D. S., 1992, *ApJ*, 392, 187
- Hatzes A. P., 1993, *ApJ*, 410, 777
- Hatzes A. P., 1995, *AJ*, 109, 350
- Henry G. W., Eaton J. A., Hamer J., Hall D. S., 1995, *ApJS*, 97, 513
- Knaack R., 1998. *Diplomarbeit, Institute of Astronomy, ETH, Zürich*
- Lockwood G. W., Skiff B. A., Baliunas S. L., Radick R. R., 1992, *Nature*, 360, 653
- Neff J. E., O’Neal D., Saar S. H., 1995, *ApJ*, 452, 879
- O’Neal D., Neff J. E., Saar S. H., 1998, *ApJ*, 507, 919
- O’Neal D., Saar S. H., Neff J. E., 1996, *ApJ*, 463, 766
- Padmakar, Pandey S. K., 1999, *A&AS*, 138, 203
- Petrovay K., 2001, in Wilson A., ed, *Proceedings of the 1st Solar & Space Weather Euroconference: The Solar Cycle and Terrestrial Climate*. ESA SP-4, p. 63
- Radick R. R., Thompson D. T., Lockwood G. W., Duncan D. K., Baggett W. E., 1987, *ApJ*, 321, 459

Radick R. R., Lockwood G. W., Skiff B. A., Baliunas S. L.,  
1998, ApJS, 118, 239

Radick R. R., Skiff B. A., Lockwood G. W., 1990, ApJ, 353, 524

Rodonò M., Messina S., Lanza A. F., Cutispoto G., Teriaca L.,  
2000, A&A, 358, 624

Saar S. H., Neff J. E., 1990, in ASP Conf. Ser. 9: Cool Stars,  
Stellar Systems, and the Sun. p. 171

Saar S. H., 1986, ApJ, 324, 441

Schrijver C. J., Title A. M., 2001, ApJ, 551, 1099

Schüssler M., Schmitt D., 2002, in Solar Variability and its  
Effect on the Earth's Atmospheric and Climate System.  
American Geophysical Union, p. 3, in press

Schüssler M., Solanki S. K., 1992, A&A, 264, L13

Schüssler M., Caligari P., Ferriz-Mas A., Solanki S. K., Stix M.,  
1996, A&A, 314, 503

Solanki S., 1992, in ASP Conf. Ser. 26: Cool Stars, Stellar  
Systems, and the Sun. p. 211

Solanki S. K., 1999, in Butler C. J., Doyle J. G., eds, ASP Conf.  
Ser. 158: Solar and Stellar Activity: Similarities and  
Differences. p. 109

Solanki S. K., 2003, A&AR, 11, 153

Steinegger M., Brandt P. N., Schmidt W., Pap J., 1990, Ap&SS,  
170, 127

Strassmeier K. G., Lupinek S., Dempsey R. C., Rice J. B., 1999,  
A&A, 347, 212

Unruh Y. C., Collier Cameron A., Cutispoto G., 1995, MNRAS,  
277, 1145

Washuettl A., Strassmeier K. G., Collier-Cameron A., 1998, in  
Donahue R., Bookbinder J., eds, Tenth Cambridge  
Workshop on Cool Stars, Stellar Systems, and the Sun. ASP  
Conference Series: 154, San Francisco, p. 2073

Washuettl A., Strassmeier K. G., Collier-Cameron A., 2001, in  
Garcia Lopez R. J., Rebolo R., Zapatero Osorio M. R., eds,  
ASP Conf. Ser. 223: 11th Cambridge Workshop on Cool  
Stars, Stellar Systems and the Sun. p. 1308